AIP | Applied Physics Letters

Towards strong light-matter coupling at the single-resonator level with sub-wavelength mid-infrared nano-antennas

M. Malerba, T. Ongarello, B. Paulillo, J.-M. Manceau, G. Beaudoin, I. Sagnes, F. De Angelis, and R. Colombelli

Citation: Applied Physics Letters **109**, 021111 (2016); doi: 10.1063/1.4958330
View online: http://dx.doi.org/10.1063/1.4958330
View Table of Contents: http://scitation.aip.org/content/aip/journal/apl/109/2?ver=pdfcov
Published by the AIP Publishing

Articles you may be interested in

Thermo-responsive mechano-optical plasmonic nano-antenna
Appl. Phys. Lett. **109**, 013109 (2016); 10.1063/1.4954907

Three-dimensional concentration of light in deeply sub-wavelength, laterally tapered gap-plasmon nanocavities
Appl. Phys. Lett. **108**, 221108 (2016); 10.1063/1.4953178

Control of the external photoluminescent quantum yield of emitters coupled to nanoantenna phased arrays
J. Appl. Phys. **118**, 073103 (2015); 10.1063/1.4928616

Remote optical sensing on the nanometer scale with a bowtie aperture nano-antenna on a fiber tip of scanning near-field optical microscopy
Appl. Phys. Lett. **106**, 151104 (2015); 10.1063/1.4918531

Optically resonant magneto-electric cubic nanoantennas for ultra-directional light scattering
J. Appl. Phys. **117**, 083101 (2015); 10.1063/1.4907536

Reuse of AIP Publishing content is subject to the terms at: https://publishing.aip.org/authors/rights-and-permissions. Download to IP: 86.252.185.79 On: Sun, 24 Jul 2016 12:29:55

Towards strong light-matter coupling at the single-resonator level with sub-wavelength mid-infrared nano-antennas

M. Malerba,[1,a)] T. Ongarello,[2,a)] B. Paulillo,[2] J.-M. Manceau,[2] G. Beaudoin,[2] I. Sagnes,[2] F. De Angelis,[1,b)] and R. Colombelli[2,c)]
[1]*Istituto Italiano di Tecnologia, Via Morego, 30, I-16163 Genova, Italy*
[2]*Centre for Nanoscience and Nanotechnology (C2N Orsay), CNRS UMR9001, Univ. Paris Sud, Univ. Paris Saclay, 91405 Orsay, France*

(Received 13 May 2016; accepted 22 June 2016; published online 13 July 2016)

We report a crucial step towards single-object cavity electrodynamics in the mid-infrared spectral range using resonators that borrow functionalities from antennas. Room-temperature strong light-matter coupling is demonstrated in the mid-infrared between an intersubband transition and an extremely reduced number of sub-wavelength resonators. By exploiting 3D plasmonic nano-antennas featuring an out-of-plane geometry, we observed strong light-matter coupling in a very low number of resonators: only 16, more than 100 times better than what reported to date in this spectral range. The modal volume addressed by each nano-antenna is sub-wavelength-sized and it encompasses only ≈4400 electrons. *Published by AIP Publishing.*
[http://dx.doi.org/10.1063/1.4958330]

Intersubband (ISB) transitions[1,2] constitute the backbone principle behind quantum cascade lasers and quantum well[3] (QW) infrared detectors. They are relevant for the study of fundamental physical phenomena at very long wavelengths such as strong light-matter coupling, non-linearities, and, more generally, cavity electrodynamics (CED). CED is in fact at the heart of fascinating phenomena such as the Purcell effect,[4] or the strong coupling regime between light and matter.[5] In the latter case, demonstrated in atoms, solid-state, and also organic systems, the light-matter coupling is stronger than any dephasing mechanism, and new system eigenstates—called polaritons[6–9] —emerge. Importantly, in the visible and near-infrared spectral ranges, it is possible to operate on isolated resonators with very high Q/V values (Q is the quality factor and V the resonator modal volume).[10] However, this is not possible in the mid-IR (10–100 THz) and in the THz (1–10 THz) because detectors are much less efficient: only *ensembles* of several hundreds/thousand cavities can be measured: the properties of the *single object* are not accessible.[3,11,12]

Here, a crucial milestone towards single-object cavity electrodynamics in the mid-IR spectral range using ultra-sub-wavelength resonators is established. We demonstrate strong light-matter coupling in the mid-IR ($\lambda \approx 9\,\mu$m) between an ISB plasmon in an n-doped semiconductor QW and the fundamental optical resonance of sub-wavelength nano-antennas in an out-of-plane configuration. An innovative nano-fabrication technology allows us to exploit two functionalities peculiar to antennas: extremely sub-wavelength field concentration and the ability to re-radiate and harvest energy efficiently.[13,14] In view of that, we achieve effective electromagnetic volumes only $V_{eff} \approx 2.4 \times 10^{-4}$ $(\lambda/n)^3$, with λ the exciting wavelength and n the effective semiconductor slab refraction index. The modal volume addressed by each nano-antenna is sub-wavelength-sized[13,15,16] and it encompasses only ≈4400 electrons. Notably, we observed strong light matter coupling at room temperature from a set of only sixteen cavities. This value is 100 times better than what reported to date,[12] opening the way, as future development, to experiments involving a single nano-resonator with possibly very few electrons involved.

Conventional optical resonators are constrained by the diffraction limit: optical confinement is limited to $\lambda_{eff}/2$ in all three dimensions of space (λ_{eff} is the wavelength within the active dielectric region), and their resonance frequency can be tuned only via the resonator size.[17] Antenna concepts have recently emerged as a way to implement otherwise inaccessible functionalities such as truly sub-wavelength 3D confinement, possibility of setting the resonance frequency independently of the resonator modal volume, and engineering of the radiation coupling.[13,15,18] These proposals are especially relevant at long wavelengths, where metals do not introduce gigantic ohmic losses and the electron kinetic inductance can be neglected.[16,19]

One of the simplest radio-frequency antennas is the vertical monopole: a straight $\lambda/4$ conductor on a metallic ground plane.[20] It is a resonant antenna which sustains resonant charge oscillations along its length that determines the operating frequency. The radiation pattern is omni-directional donut-like-shaped with peak-radiation parallel to the ground plane. Recent fabrication technologies[21,22] (Fig. 1) permit to extend this concept to the mid-infrared spectral range. As described in Fig. 1(a), by adapting the methods described in Ref. 21 we have inserted an ultra-thin semiconductor QW active region between an out-of-plane gold nano-antenna and its metallic ground plane (see description in the supplementary material[23]). The advantages are many-fold. First, the electric field is *squeezed* to deep sub-wavelength dimensions between the lower antenna tip and the ground plane. Importantly, the electric field is orthogonal to the QW layers

[a)]M. Malerba and T. Ongarello contributed equally to this work.
[b)]E-mail: francesco.deangelis@iit.it
[c)]E-mail: raffaele.colombelli@u-psud.fr

Reuse of AIP Publishing content is subject to the terms at: https://publishing.aip.org/authors/rights-and-permissions. Download to IP: 86.252.185.79 On: Sun, 24 Jul 2016 12:29:55

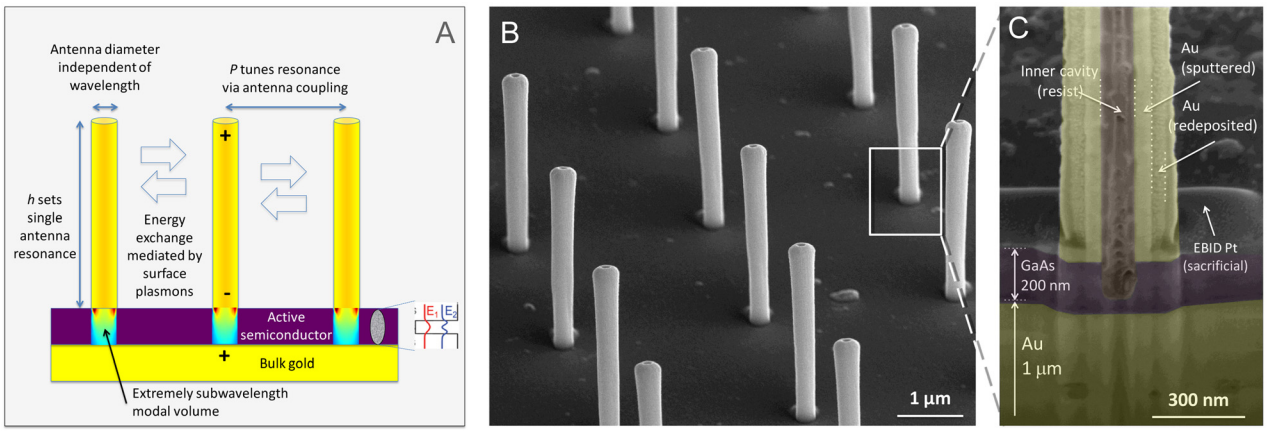

FIG. 1. (a) Cross-sectional scheme of the device. The semiconductor QW slab rests on a thick gold surface. The nano-antennas are fabricated on top of the semiconductor slab that is composed—as schematized—by semiconductor QWs. In the fundamental antenna resonance charges oscillate along the rod's main axis, as schematized for the central element. (b) SEM image of a typical final nano-antenna array. (c) Colored cross-section of the antenna foot, which here was cut by FIB.

and couples efficiently with the ISB dipole. Figure 1(b) shows a scanning electron microscopy (SEM) image of an array of nano-antennas. Figure 1(c) shows a cross-section of the antenna foot that highlights the sub-wavelength modal volume achievable. Second, the operating wavelength is determined by the vertical height h of the antennas (and, for arrays, the antenna distance P) and is no longer correlated with the modal volume which depends only on the antenna cross section. Finally, owing to their omni-directional radiation pattern in the xy plane, energy is re-radiated toward the neighboring array elements, enabling an efficient radiation harvesting effect.[24]

Figure 2(a) shows the simulated reflectivity of an array of nano-antennas ($h = 3.1\,\mu$m and $P = 3.5\,\mu$m) on a 175 nm thick undoped semiconductor slab. The fundamental antenna resonance, which provides maximum field confinement, appears as a sharp reflectivity dip at a frequency $f_{antenna} \approx 35$ THz, with relatively flat dispersion at incidence angles $\theta < 35/40°$. The operating frequency is also tailorable via the array period, as shown also in the supplementary material[23] (Fig. S2). The effect is reported in Ref. 14, albeit for antennas on a metallic ground plane. Its physical origin lies in an energy exchange between the nano-antennas and the surface-plasmon propagating at the metal–semiconductor–air interface. Since the monopolar nano-antennas re-radiate energy efficiently, the coupling is strong and it affects the resonance frequency even in the nondispersive region close to $k = 0$ (see the supplementary material[23]). An additional benefit is an increased Q-factor, since each nano-antenna re-captures the radiation emitted by the nearby ones, which would be otherwise lost.[24] The experimental Q-factor of a single nano-antenna is typically 5, while in the array configuration it ranges from 10 to 25.[14]

We have fabricated arrays of nano-antennas, placing them on three different semiconductor QW samples: D0 (no doping), D2 (low doping, $6.3 \times 10\,\text{cm}^{-2}$), and D10 (high doping, $1.85 \times 10^{13}\,\text{cm}^{-2}$). The samples had been previously waferbonded to a thick gold layer evaporated on a GaAs carrier substrate. Figure 2(b) shows the samples' absorption measured in a multi-pass geometry (before waferbonding) at room temperature: D0 (reference sample) does not absorb, while D2 and D10 exhibit absorptions at $\lambda \approx 9.7$ (30.9 THz) and $\lambda \approx 9\,\mu$m (33.3 THz), respectively. The resonances stem from ISB transitions between the quantized QW electronic levels. The semiconductor slabs are very thin (151 nm D0

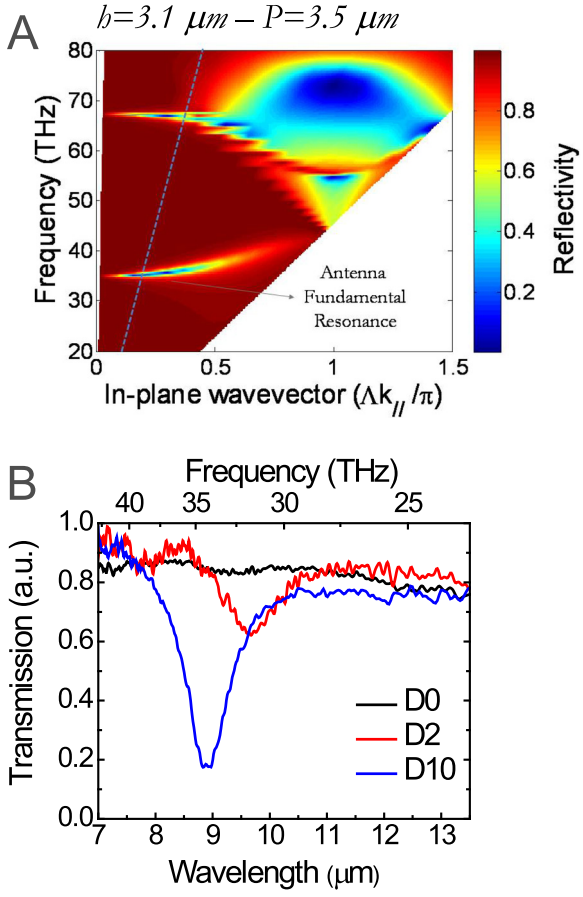

FIG. 2. (a) Numerically simulated frequency vs wavevector band diagram of an array ($h = 3.1\,\mu$m and $P = 3.5\,\mu$m) of nano-antennas on a semi-insulating GaAs slab. The color-bar represents the reflectivity. The dotted blue line corresponds to an incidence angle of 15°. The simulation has been performed with a commercial software (Comsol Multiphysics). Dispersive $\varepsilon(\omega)$ for metal[16] and GaAs[33] was employed (supplementary material[23]). (b) Room temperature ISB absorption for samples D0, D2, and D10 measured in a multipass waveguide configuration. D0, the reference sample, does not absorb. D2 and D10 exhibit a clear resonance at $\lambda = 9.4\,\mu$m and $\lambda = 9\,\mu$m, respectively.

Reuse of AIP Publishing content is subject to the terms at: https://publishing.aip.org/authors/rights-and-permissions. Download to IP: 86.252.185.79 On: Sun, 24 Jul 2016 12:29:55

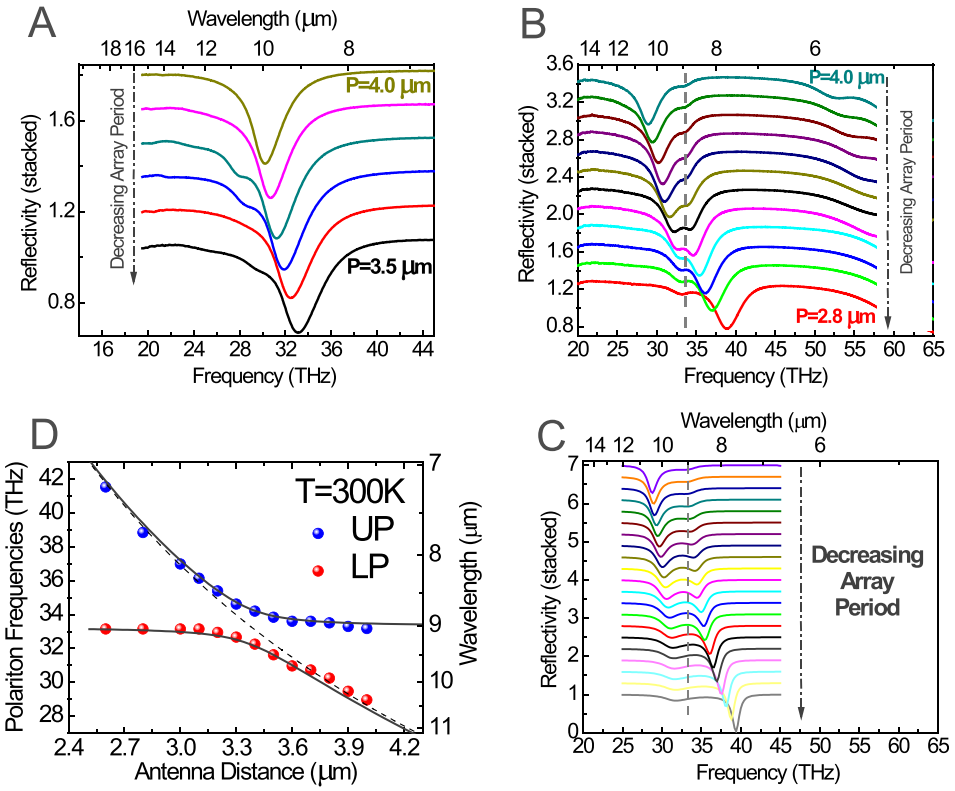

FIG. 3. (a) Reflectivity spectra of sample D10 after the first gold deposition (step B in Fig. S1). The whole sample surface is metal-covered. The fundamental nano-antenna mode tunes with the array period. The spectra have been acquired with a Nicolet FTIR coupled to a microscope. The measurement spot is 60 × 60 μm^2 and the detection is performed with a liquid-nitrogen cooled MCT detector. (b) Reflectivity spectra of sample D10 after the Ar-milling step that uncovers the semiconductor surface (step C in Fig. S1) and permits the coupling of the ISB excitation with the nano-antenna mode. Several values of P have been implemented to tune the antenna mode in and out of the bare ISB resonance, marked by the grey dotted line. A clear anticrossing behavior is observed. (c) Numerically simulated reflectivity of sample D10 as a function of the array period P. The nano-antenna height is 3.1 μm. (see the supplementary material for the numerical details). The polaritonic anticrossing behavior is correctly reproduced. A larger Rabi splitting (3.7 THz) with respect to the measurements (2 THz) is obtained. (d) UP and LP energies—obtained from the reflectivity measurements—as a function of the array period (blue and red dots). A Rabi splitting value of ≈2 THz is measured. The continuous grey lines are the solutions of the secular equation (2) with no fitting parameters. The grey dotted line is the frequency of the empty cavity resonance.

and D2; 171 nm D10), and after waferbonding and substrate removal, they rest on a metallic ground plane (scheme in Fig. 1(a)), ready for nano-antenna implementation.

The final devices consist of 3.1-μm-high nano-antennas with periods P in the 2.5–4 μm range. The optical characterizations are performed in reflectivity (details are given in the supplementary material[23]). We first measure the devices at an intermediate fabrication step (Fig. S1-B) when the gold metallization covers antennas *and* semiconductor slab; hence, no light-matter coupling is possible. The results for different periods P are reported in Fig. 3(a). They agree with the simulations: the resonance lies in the 30–35 THz range and frequency-tunes with P.

The final fabrication step (Ar^+ milling, Fig. S1-C) selectively removes the metal covering the semiconductor QWs, without attacking the antenna sidewalls: the coupling between antenna resonance and ISB excitation is now possible. Figure 3(b) reports the measurements on sample D10: the nano-antenna resonance is frequency tuned in and out of the ISB transition marked by the vertical dotted gray line. An anti-crossing behavior is observed, proving that we operate in the strong-coupling regime between light and matter. We can thus associate the observed peaks to the lower (LP) and upper polariton (UP) states. Identical measurements performed on the reference sample D0 (Fig. S4) only show one peak and provide a consistency check.

Figure 3(c) shows the numerically simulated reflectivity of sample D10, in agreement with the experimental data in panel B. Figure 3(d) reports the energy positions of the LP and UP peaks as a function of the array period P. The minimum anticrossing energy, the vacuum field Rabi splitting, is ≈2 THz, at the onset of the strong-coupling regime. The data permit to estimate the modal optical confinement factor. The vacuum Rabi splitting is twice the Rabi frequency and can be expressed—in a simplified approximation—as follows[25,26] (the exact formulation is in Ref. 27):

$$2\Omega_{Rabi} = \sqrt{\Gamma_{opt} \cdot f_w}\omega_{plasma} = \sqrt{\Gamma_{opt} \cdot f_w} \cdot \sqrt{\frac{f_{12} e^2 n_{2D}}{\varepsilon_0 \varepsilon_{slab} m^* L_{QW}}}. \quad (1)$$

Γ_{opt} is the mode optical confinement factor; f_w is the QW overlap factor (defined as the ratio between the sum of the thickness of all the QWs and the total sample thickness); ω_{plasma} the plasma frequency of the electrons in the QW; f_{12} the ISB transition oscillator strength; e the electron charge; n_{2D} the electronic surface density; ε_{slab} the semiconductor dielectric constant; m^* the electronic effective mass; and L_{QW} the QW thickness. f_w and ω_{plasma} are estimated from the nominal sample characteristics. In our case, this yields $f_w = 11\%$. The choice for ω_{plasma} is detailed in the supplementary material.[23] Using these values, the estimated modal

Reuse of AIP Publishing content is subject to the terms at: https://publishing.aip.org/authors/rights-and-permissions. Download to IP: 86.252.185.79 On: Sun, 24 Jul 2016 12:29:55

optical confinement factor is $\Gamma_{opt} \approx 3\%$, in fair agreement with numerical simulations predicting 3.7%. This value is much lower than what is achievable with patch cavities[28] or loop-antenna LC resonators[15] but is the "price to pay" to achieve extremely sub-wavelength confinement without excessive ohmic losses, as elucidated in Ref. 16, and—in perspective—to operate the system with few electrons involved. The continuous lines in Fig. 3(d) are the roots of the following secular equation:

$$(\omega^2 - \omega^2_{antenna}) \cdot (\omega^2 - \omega^2_{12}) = \Gamma_{opt}\omega^2_{plasma}\omega^2_{antenna}, \quad (2)$$

which correspond to the frequencies of the UP and LP states.[25] $\omega_{antenna}$ is the frequency of the antenna resonance (dashed grey line) and it is tuned with P, and ω_{12} is the experimental ISB transition frequency. The general trend is correctly reproduced, especially the value of the Rabi splitting.

Figure 4 shows the numerically calculated field distributions of the relevant nano-antenna mode. The mode almost totally overlaps with the active region, and it is localized below the antenna foot. In particular, given the hollow cylinder shape of the antenna, the active volume—i.e., the volume where the electromagnetic field of the antenna mode is localized—has a toroidal shape, defined by the inner antenna diameter (≈100 nm) and the outer antenna diameter (≈200 nm). We can therefore estimate the modal volume as surface of the antenna toroidal foot *by* active region thickness, which yields a value of $4.12 \times 10^{-3}\,\mu m^3$. Figure 4(b) also reveals that Γ_{opt} is small because the field is also present at the other antenna's end. The antenna being in air ($\varepsilon = 1$), while $\varepsilon_{GaAs} = 13$, the overlap is low. Embedding the nano-antennas in high-index material is an optimal strategy to increase Γ_{opt}.[29]

The measured devices contain 600 to 900 nano-antenna elements (25 × 25 up to 30 × 30), a large number, albeit already inferior to the current lower limit.[12] We now show that it is possible to reduce the resonator number by almost 2 orders of magnitude. We have realized small arrays on

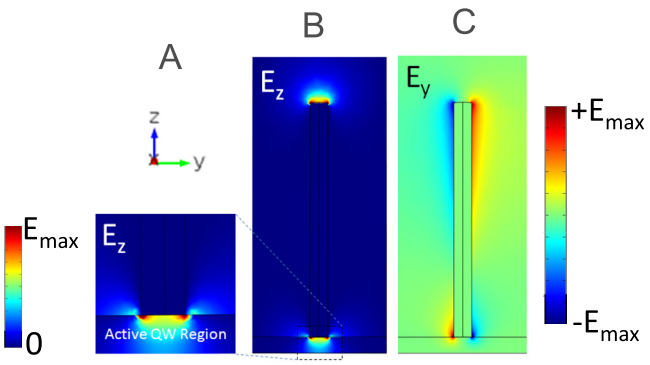

FIG. 4. (a) Numerical simulation of the field distribution of the z-component of the electric field at the nano-antenna fundamental resonance (E_z is plotted). The field is mainly localized at the antenna edges, as expected from the tip effect in electrostatics. (b) Close up of the antenna foot: the electric field is mainly localized below the antenna. (c) Numerical simulation of the field distribution of the y-component of the electric field. The fundamental mode presents only one field node at approximately half the antenna length, thus explaining the low radiative Q-factor which is a key to the light-harvesting properties of this system.[31]

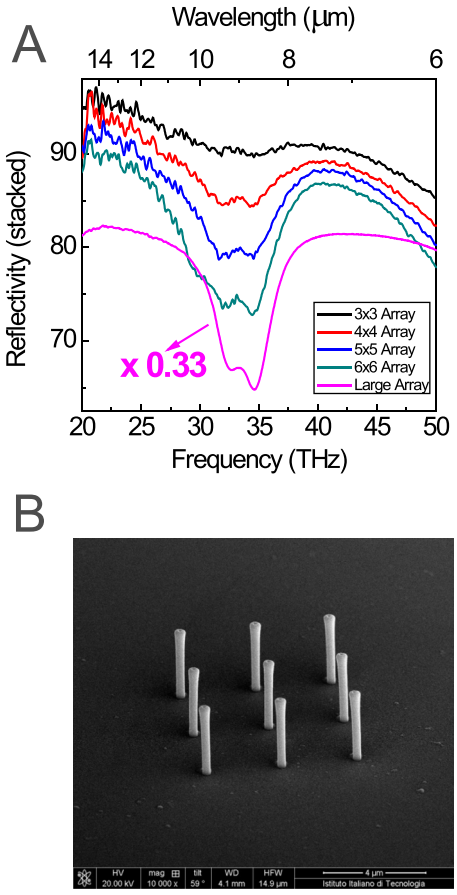

FIG. 5. (a) Reflectivity spectra of sample D10 when the ISB excitation couples with the nano-antenna mode, using arrays containing a small number of antennas. P is 3.3 μm. We can observe the UP and LP states down to an array containing only 16 nano-antennas (thick red solid line). The 3 × 3 array does not permit to identify the polaritonic modes, possibly because the array Q-factor starts to drop. (b) SEM image of the 3 × 3 nano-antenna array. Its total lateral size is only ≈7 μm, while the microscope spot—for the reflectivity spectrum—is ≈20 × 20 μm^2.

sample D10, from 6 × 6 (36 elements) down to 3 × 3 (9 elements, Fig. 5(b)). The experimental reflectivity is reported in Fig. 5(a), for the zero detuning case ($h = 3.1\,\mu$m and $P = 3.3\,\mu$m). The Rabi splitting does not change with the resonator number, thus proving that the CED effect happens at the single resonator level. Importantly, we observe a splitting down to 16 resonators only (4 × 4 array), approximately 100 times better than that previously reported.[12] (Note: in a different system based on superconducting resonators at 4 K in magnetic fields, a hundred or more resonators only can be measured.[30] We improve one order of magnitude in comparison to that system too).

The 4 × 4 array is ≈10–μm-wide, with a focusing spot ≈20-μm-wide. Since the fully illuminated large arrays absorb ≈50% of the light, scaling with the ratio of the array over the spot surface yields a contrast of ≈12.5%. The measured value of ≈6% is compatible with this simple scaling law. The nano-antennas, however, are exceptionally effective in capturing light: they cover approximately 3.5% of the sample surface, but absorb 50% of the incident light. The origin is twofold. On the one hand, each nano-antenna re-radiates energy towards the neighboring array elements, enabling an efficient radiation harvesting.[24] Furthermore, the

Reuse of AIP Publishing content is subject to the terms at: https://publishing.aip.org/authors/rights-and-permissions. Download to IP: 86.252.185.79 On: Sun, 24 Jul 2016 12:29:55

magneto-electric interference (MEI) effect,[31] which explains the funneling of optical energy into subwavelength grooves etched on a metallic surface,[32] may play a role. For a scattering object on a metallic surface, one term (S_{MEI}) of the Poynting vector is proportional to $E_s \times H_i$, with H_i the magnetic field of the incoming wave and E_s the electric field of the waves scattered by the nano-antenna. The energy flux of S_{MEI} converges from the surface towards the antenna, effectively enabling energy harvesting over a larger surface. Our nano-antennas behave as *vertical* dipoles and re-radiate energy efficiently as cylindrical waves bound to the metallic ground plane. The $Q_{radiative}$ of a single antenna is 10, similar to Q_{ohmic}, correctly yielding 5 for the experimentally measured Q_{total}. As a result, E_s is high in our system, and the magneto-electric interference effect is very efficient. This is in contrast with resonators that behave as *horizontal* dipoles: the out-of-plane geometry therefore enables operation at the almost single-resonator level.

In conclusion, we demonstrated cavity electrodynamics in the mid-infrared at the almost single-object level, by observing strong light-matter coupling between an intersubband transition in a semiconductor QW and a set of only sixteen ultra-sub-wavelength resonators. In each resonator, only ≈4400 electrons are involved in the light-matter process. There are numerous perspectives of this result. A further reduction in the resonator number to the ultimate limit of one is possible, by leaving the active semiconductor material in place under the central post only. Proper optimization of the nano-antenna will permit operation with an extremely small number of electrons (around or below the hundreds), thus enabling access—for instance—to photon blockade processes. As more immediate perspectives, non-linear optical processes with low incident powers are at hand given the field enhancements available and also the extension of this architecture to the THz. Finally, the low number of resonators can potentially enable device integration in more complex opto-electronic chips, such as detectors.

We thank Adel Bousseksou and Stefano Pirotta for useful discussions and careful reading of the manuscript. This work was partly supported by the French RENATECH network. R.C. and T.O. acknowledge support from the ERC "GEM" grant (Grant Agreement No. 306661). F.D.A. acknowledges support from ERC "Neuro-Plasmonics" (Ideas Program, Grant Agreement No. 616213).

[1]E. R. Weber, R. K. Willardson, H. C. Liu, and F. Capasso, *Intersubband Transitions in Quantum Wells: Physics and Device Applications: Physics and Device Applications* (Academic Press, 1999).
[2]D. Dini, R. Kohler, A. Tredicucci, G. Biasiol, and L. Sorba, Phys. Rev. Lett. **90**, 116401 (2003).
[3]A. Delteil, A. Vasanelli, Y. Todorov, C. Feuillet Palma, M. Renaudat St-Jean, G. Beaudoin, I. Sagnes, and C. Sirtori, Phys. Rev. Lett. **109**, 246808 (2012).
[4]E. Purcell, Phys. Rev. **69**, 681 (1946).
[5]C. Cohen-Tannoudji, J. Dupont-Roc, and G. Grynberg, *Photons and Atoms* (Wiley-VCH Verlag GmbH, Weinheim, Germany, 1997).
[6]C. Weisbuch, M. Nishioka, A. Ishikawa, and Y. Arakawa, Phys. Rev. Lett. **69**, 3314 (1992).
[7]J. P. Reithmaier, G. Sek, A. Loffler, C. Hofmann, S. Kuhn, S. Reitzenstein, L. V. Keldysh, V. D. Kulakovskii, T. L. Reinecke, and A. Forchel, Nature **432**, 197 (2004).
[8]A. E. Schlather, N. Large, A. S. Urban, P. Nordlander, and N. J. Halas, Nano Lett. **13**, 3281 (2013).
[9]T. Schwartz, J. A. Hutchison, C. Genet, and T. W. Ebbesen, Phys. Rev. Lett. **106**, 196405 (2011).
[10]B. Deveaud, *The Physics of Semiconductor Microcavities* (John Wiley & Sons, 2007).
[11]M. Geiser, F. Castellano, G. Scalari, M. Beck, L. Nevou, and J. Faist, Phys. Rev. Lett. **108**, 106402 (2012).
[12]A. Benz, S. Campione, S. Liu, I. Montano, J. F. Klem, A. Allerman, J. R. Wendt, M. B. Sinclair, F. Capolino, and I. Brener, Nat. Commun. **4**, 2882 (2013).
[13]C. Walther, G. Scalari, M. I. Amanti, M. Beck, and J. Faist, Science **327**, 1495 (2010).
[14]M. Malerba, A. Alabastri, E. Miele, P. Zilio, M. Patrini, D. Bajoni, G. C. Messina, M. Dipalo, A. Toma, R. P. Zaccaria, and F. De Angelis, Sci. Rep. **5**, 16436 (2015).
[15]B. Paulillo, J. M. Manceau, A. Degiron, N. Zerounian, G. Beaudoin, I. Sagnes, and R. Colombelli, Opt. Express **22**, 21302 (2014).
[16]J. B. Khurgin, Nat. Nanotechnol. **10**, 2 (2015).
[17]B. E. A. Saleh and M. C. Teich, *Fundamentals of Photonics*, 2nd ed. (Wiley, 2007).
[18]E. Strupiechonski, G. Xu, M. Brekenfeld, Y. Todorov, N. Isac, A. M. Andrews, P. Klang, C. Sirtori, G. Strasser, A. Degiron, and R. Colombelli, Appl. Phys. Lett. **100**, 131113 (2012).
[19]M. A. Ordal, L. L. Long, R. J. Bell, S. E. Bell, R. R. Bell, R. W. Alexander, Jr., and C. A. Ward, Appl. Opt. **22**, 1099 (1983).
[20]C. A. Balanis, Proc. IEEE **80**, 7 (1992).
[21]F. De Angelis, M. Malerba, M. Patrini, E. Miele, G. Das, A. Toma, R. P. Zaccaria, and E. Di Fabrizio, Nano Lett. **13**, 3553 (2013).
[22]P. Zilio, M. Malerba, A. Toma, R. P. Zaccaria, A. Jacassi, and F. De Angelis, Nano Lett. **15**, 5200 (2015).
[23]See supplementary material at http://dx.doi.org/10.1063/1.4958330 for sample details and fabrication; additional reflectivity measurements; analytical fit of LP/UP energies; and numerical simulations and array operating principle.
[24]R. Adato, A. A. Yanik, C.-H. Wu, G. Shvets, and H. Altug, Opt. Express **18**, 4526 (2010).
[25]Y. Todorov, A. M. Andrews, R. Colombelli, S. De Liberato, C. Ciuti, P. Klang, G. Strasser, and C. Sirtori, Phys. Rev. Lett. **105**, 196402 (2010).
[26]C. Ciuti, G. Bastard, and I. Carusotto, Phys. Rev. B **72**, 115303 (2005).
[27]Y. Todorov and C. Sirtori, Phys. Rev. B **85**, 045304 (2012).
[28]R. Esteban, T. V. Teperik, and J. J. Greffet, Phys. Rev. Lett. **104**, 026802 (2010).
[29]W. Zhou and T. W. Odom, Nat. Nanotechnol. **6**, 423 (2011).
[30]C. Maissen, G. Scalari, F. Valmorra, M. Beck, J. Faist, S. Cibella, R. Leoni, C. Reichl, C. Charpentier, and W. Wegscheider, Phys. Rev. B **90**, 205309 (2014).
[31]F. Pardo, P. Bouchon, R. Haïdar, and J.-L. Pelouard, Phys. Rev. Lett. **107**, 093902 (2011).
[32]T. Thio, K. M. Pellerin, R. A. Linke, H. J. Lezec, and T. W. Ebbesen, Opt. Lett. **26**, 1972 (2001).
[33]E. D. Palik, *Handbook of Optical Constants of Solids* (Elsevier, 1985).

Reuse of AIP Publishing content is subject to the terms at: https://publishing.aip.org/authors/rights-and-permissions. Download to IP: 86.252.185.79 On: Sun, 24 Jul 2016 12:29:55